Journal of Turbomachinery

Copy of e-mail Notification

Journal of Turbomachinery Published by ASME
Dear Author,

Congratulations on having your paper accepted for publication in the ASME Journal Program.
Your page proof is available in PDF format from the ASME Proof Download & Corrections site here:
http://115.111.50.156/jw/AuthorProofLogin.aspx?pwd=dea0169a7da9

Login: your e-mail address
Password: dea0169a7da9

Please keep this email in case you need to refer back to it in the future.
You will need Adobe Acrobat Reader software to view the file. This is free software and a download link is provided when you log in to view your proofs.

Responsibility of detecting errors rests with the author. Please review the page proofs carefully and:

1. Answer any queries on the first page “Author Query Form”
2. Proofread any tables and equations carefully
3. Check to see that any special characters have translated correctly
4. Publication will not proceed until a response is received. If there are no corrections, a response is still required.

RETURNING CORRECTIONS:
Corrections must be returned using the ASME Proof Download & Corrections Submission Site (link above). You will be able to upload:

1. Annotated PDF
2. Text entry of corrections, with line numbers, in the text box provided
3. Additional files, if necessary.

SPECIAL NOTES:
Your Login and Password are valid for a limited time. Please reply within 48 hours.

Corrections not returned through the above website will be subject to publication delays.
This e-proof is to be used only for the purpose of returning corrections to the publisher.
If you have any questions, please contact: asme.cenveo@cenveo.com, and include your article no. (TURBO-14-1160) in the subject line. This email should not be used to return corrections.

Sincerely,
Mary O'Brien, Journal Production Manager

STATEMENT OF EDITORIAL POLICY AND PRACTICE

The Technical Committee on Publications and Communications (TCPC) of ASME aims to maintain a high degree of technical, literary, and typographical excellence in its publications. Primary consideration in conducting the publications is therefore given to the interests of the reader and to safeguarding the prestige of the Society.

To this end the TCPC confidently expects that sponsor groups will subject every paper recommended by them for publication to careful and critical review for the purpose of eliminating and correcting errors and suggesting ways in which the paper may be improved as to clarity and conciseness of expression, accuracy of statement, and omission of unnecessary and irrelevant material. The primary responsibility for the technical quality of the papers rests with the sponsor groups.

In approving a paper for publication, however, the TCPC reserves the right to submit it for further review to competent critics of its own choosing if it feels that this additional precaution is desirable. The TCPC also reserves the right to request revision or condensation of a paper by the author or by the staff for approval by the author. It reserves the right, and charges the editorial staff, to eliminate or modify statements in the paper that appear to be not in good taste and hence likely to offend readers (such as obvious advertising of commercial ventures and products, comments on the intentions, character, or acts of persons and organizations that may be construed as offensive or libelous), and to suggest to authors rephrasing of sentences where this will be in the interest of clarity. Such rephrasing is kept to a minimum.

Inasmuch as specific criteria for the judging of individual cases cannot, in the opinion of the TCPC, be set up in any but the most general rules, the TCPC relies upon the editorial staff to exercise its judgment in making changes in manuscripts, in rearranging and condensing papers, and in making suggestions to authors. The TCPC realizes that the opinions of author and editor may sometimes differ, and hence it is an invariable practice that no paper is published until it has been passed on by the author. For this purpose page proofs of the edited paper are sent to the author prior to publication in a journal. Changes in content and form made in the proofs by authors are followed by the editor except in cases in which the Society's standard spelling and abbreviation forms are affected.

If important differences of opinion arise between author and editor, the points at issue are discussed in correspondence or interview, and if a solution satisfactory to both author and editor is not reached, the matter is laid before the TCPC for adjustment.

Technical Committee on Publications and Communications (TCPC)
Reviewed: 05/2012

AUTHOR QUERY FORM

ASME SETTING THE STANDARD	**Journal: J. Turbomach.** **Article Number: TURBO-14-1160**	**Please provide your responses and any corrections by annotating this PDF and uploading it to ASME's eProof website as detailed in the Welcome email.**

Dear Author,

Below are the queries associated with your article; please answer all of these queries before sending the proof back to Cenveo. Production and publication of your paper will continue after you return corrections or respond that there are no additional corrections.

Location in article	Query / Remark: click on the Q link to navigate to the appropriate spot in the proof. There, insert your comments as a PDF annotation.
AQ1	As per journal style, three or fewer letter acronyms does not allow in the title; therefore, we have replaced the acronym CFD with the spelled out definition. Please check and confirm.
AQ2	Please provide zip code for all the affiliations.
AQ3	Please provide report number for Ref. 1.
AQ4	Please provide required information for Refs. 2, 4, 17, 18, and 24.
AQ5	Please provide DOI for Refs. 3, 6 and 7.
AQ6	Please provide issue number for Ref. 23.

Thank you for your assistance.

Quantitative Computational Fluid Dynamic Analyses of Particle Deposition on a Transonic Axial Compressor Blade—Part II: Impact Kinematics and Particle Sticking Analysis

AQ2

Alessio Suman
Dipartimento di Ingegneria,
Università degli Studi di Ferrara,
Ferrara ■, Italy

Mirko Morini
Dipartimento di Ingegneria Industriale,
Università degli Studi di Parma,
Parma ■, Italy

Rainer Kurz
Solar Turbines Incorporated,
San Diego, CA ■

AQ1

Nicola Aldi
Dipartimento di Ingegneria,
Università degli Studi di Ferrara,
Ferrara ■, Italy

Klaus Brun
Southwest Research Institute,
San Antonio, TX ■

Michele Pinelli
Dipartimento di Ingegneria,
Università degli Studi di Ferrara,
Ferrara ■, Italy

Pier Ruggero Spina
Dipartimento di Ingegneria,
Università degli Studi di Ferrara,
Ferrara ■, Italy

In heavy-duty gas turbines, the microparticles that are not captured by the air filtration system can cause fouling and, consequently, a performance drop of the compressor. This paper presents three-dimensional numerical simulations of the microparticle ingestion (0 μm–2 μm) on an axial compressor rotor carried out by means of a commercial computational fluid dynamic (CFD) code. Particle trajectory simulations use a stochastic Lagrangian tracking method that solves the equations of motion separately from the continuous phase. The NASA Rotor 37 is considered as a case study for the numerical investigation. The compressor rotor numerical model and the discrete phase model were previously validated by the authors in the first part of this work. The kinematic characteristics (velocity and angle) of the impact of micrometric and submicrometric particles with the blade surface of an axial transonic compressor are shown. The blade zones affected by particle impact were extensively analyzed and reported in the first part of this work, forming the starting point for the analyses shown in this paper. The kinematic analysis showed a high tendency of particle adhesion on the suction side (SS), especially for the particles with a diameter equal to 0.25 μm. Fluid dynamic phenomena and airfoil shape play a key role regarding particle impact velocity and angle. This work has the goal of combining, for the first time, the kinematic characteristics of particle impact on the blade with fouling phenomenon by the use of a quantity called sticking probability (SP) adopted from literature. From these analyses, some guidelines for a proper management of the power plant (in terms of filtration and washing strategies) are highlighted. [DOI: 10.1115/1.4028296]

Introduction

Ambient air is a continuous medium that contains and carries a large number of particles (contaminants). The contaminants in the air are different in composition, size (pollen of 50 μm, spores of 3 μm–10 μm, and exhaust particle < 0.1 μm), and quantity [1].

The quality and purity of the air entering the turbine is a significant factor in the performance and life of the gas turbine. Therefore, air inlet filtration systems are employed to remove a significant amount of the contaminants. Fouling of axial compressors (caused by particles smaller than 2 μm) is a serious operating problem and its control is of critical importance for operators of gas turbine driven power plants, compressor stations, and pump stations.

Estimates have cited fouling as being responsible for 70% to 85% of all gas performance losses accumulated during operation. Output losses between 2% (under favorable conditions) and 15–20% (under adverse conditions) have been experienced [2]. In order to minimize the performance loss of the turbines in the power plant, an adequate filtration system that can limit the ingestion of contaminants by the power unit is required.

Although 99% of the particles in the atmosphere are less than 1 μm in size, 70% of the weight is due to particles which have a diameter greater than 1 μm [3]. In order to capture these different types of particles, filtration systems use many different mechanisms. Each filter in fact has various different mechanisms working together to remove the particles. An extensive report on filtration efficiency can be found in Ref. [4] where it can be seen that for the particles with dimensions less than ≈2 μm, and in more detail, with diameters in the range of 0.1 μm–1.0 μm, conventional filtration systems will not entirely prevent these small particles from entering the gas turbine and therefore may cause fouling.

The details on how the small particles entering the gas turbine reach the blade surface and stick there are not fully and quantitatively understood. Particle adhesion on the blade surface is a complex phenomenon that includes many aspects that can be summarized as follows:

– the material of the body in contact (blade and particle): density, ultimate strength, and elastic yield limit (in order to define an elastic or plastic collision);
– the surface conditions: roughness, presence of added materials (water, oil, and grease), presence of electrostatic charges or its generation by contact (bounces or slips) with the particles;
– the particle size: inertia force and some energy whose effects are directly related to particle size [5];

Contributed by the International Gas Turbine Institute (IGTI) of ASME for publication in the Journal of Turbomachinery. Manuscript received July 21, 2014; final manuscript received August 4, 2014; published online xx xx, xxxx. Editor: Ronald Bunker.

- the impact velocity is directly related to kinetic energy. This energy is transferred into the contact zone between two bodies and determines deformation, bounce, and sometimes particle breakage;
- the impact angle represents the most important quantity for impact kinematics and consequent impact effects (bounce, adhesion, or slip).

All these phenomena can be studied from many points of view: (i) kinematic (velocity and direction), (ii) dynamic (velocity and mass), and (iii) energy (deformations or breaks). At the same time, it is possible to consider microscopic effects (e.g., atoms attractions and molecular bonds) or macroscopic (e.g., adhesion, rebounds, and deformations).

In almost all cases, the phenomena mentioned above occur at the same time during the contact between two bodies and the result of the contact depends on the combination of these effects.

Particle sticking on blade surfaces results in an increase of the thickness of the airfoil and the surface roughness. Both of these events change the flow path inside the passage vanes. This leads to in particular: (i) an increment of boundary layer thickness, (ii) a decrement of the flow passage area, and (iii) modifications of 3D fluid dynamic phenomena.

In this paper, the kinematic characteristics of the submicrometric and micrometric particles (0.25 μm–2.00 μm) that impact on an axial compressor blade will be shown and explained. The particle collision results are reported in Ref. [6] and represent the starting point of this work.

Literature Review

The interaction between two bodies, with or without the action of an external force, has been a subject of study since the 19th century. The first comprehensive study on the mechanical impact between two bodies was conducted by Hertz in 1882 [7]. The classic approach to this type of problem consists in most cases of description of the impact (usually normal impacts) phenomena which involves two bodies (usually sphere–sphere or sphere–surface) made from a ductile material that has a defined yield load. In this case, the deformation of the bodies plays a key role during contact and determines the result of the impact.

One of the major contributions to this field has been provided by Johnson, Kendall, and Roberts (JKR) [8]. The JKR model describes the phenomena that occur between two bodies in contact demonstrating that even if there is not an external force maintaining two bodies in contact, there is a well-defined contact area at the body interface and it requires a force greater than zero to separate it. Based on the JKR method, many authors have described contact models based on experimental or analytic results in order to make predictions and estimates regarding the impact behaviors of two bodies.

Thorton and Ning [9], for example, have formulated a model of rebound/adhesion which takes into account impact velocity, capture velocity, and yield velocity. Capture velocity represents the particle velocity limit below which contact becomes adhesion and above which contact becomes rebound. Yield velocity represents the material particle velocity limit below which impact can be considered elastic and above which a plastic deformation occurs in the contact zone. Yield velocity is a function of the materials (Young's module, Poisson's ratio, and density). The authors also performed a study on the influence of the energy at the interface and demonstrated that for the highest velocity impact the energy interface does not affect the values of restitution coefficients.

One of the most important experimental reports was provided by Wall et al. [10]. The authors have performed a number of experiments with ammonium fluorescein microspheres (with diameters equal to 2.58 μm, 3.44 μm, 4.90 μm, and 6.89 μm) impacted normally against smooth, flat surfaces of polished molybdenum, silicon, cleaved mica, and a fluorocarbon polymer over an initial velocity up to 100 m/s. The main results shown in this work can be summarized as follows: (i) at low velocity (<20 m/s), the ratio of rebound to impact velocity was sensitive to target material, decreasing with impact velocity due to the adhesion surface energy, (ii) the kinetic energy recovered in low velocity impacts was found to depend on particle size, (iii) no such particle size dependence was observed for impact velocities near 20 m/s, and (iv) above 40 m/s, the velocity ratio was insensitive to the target material, indicating that the particle has a lower elastic yield limit than the material target. Finally, the authors have highlighted that the plastic deformation was a significant component of energy loss at all impact velocities and the knowledge of interface energy plays a key role for the proper description of particle impact.

Unfortunately, most of the models and the results reported in literature do not provide a full understanding of the adhesion phenomena which is responsible for the fouling mechanism. This limit is largely due to (i) different particle sizes, (ii) different material characteristics (some particle materials do not show the elastic yield limit), and (iii) the different impact velocity. In fact, if the model reported in Ref. [9] is applied to a metallic micro-sized particle with Young's module equal to 72 GPa, Poisson's ratio equal to 0.17, and a surface energy equal to 0.2 J/m^2; the capture velocity is approximately 1 m/s. By using these results for fouling phenomena and considering that the submicrometric and micrometric particles follow the streamline with a velocity of about 350 m/s, all of these particles must bounce on the blade surface and the fouling phenomena would not exist.

Some very interesting results and detailed analysis of microparticle adhesion can be found in astrophysics applications related to the research of preplanetary dust dynamics. The particles, in most cases consisting of submicrometric silica spheres, are the basis of the planets' origin. These space-dispersed particles collide with each other, and if the impact allows for adhesion, the particles generate an agglomerate. The difference between these mechanisms, not yet fully understood and the fouling phenomenon, is due to the type of motion. In fact, the preplanetary particles move in cosmic space, characterized by high Knudsen numbers (molecular motion), while in the case of fouling, and more generally of motions in the Earth's atmosphere, the transportation of the particles takes place with very small Knudsen numbers (viscous motion). This aspect must not diminish the importance of the results highlighted in this research field because the experiments are conducted only in some cases under vacuum and the results are often in line with the more classical theories mentioned above. The uniqueness and usefulness of these studies are that the particle velocities, materials, and dimensions are in the same range as those responsible for the fouling phenomenon.

In this field of research, one of studies closest to the fouling phenomena is Ref. [11], reporting experimental evaluations of perfectly spherical and irregular particles impacting a smooth surface (smooth as the particle surface). Different combinations of particle size and materials have been tested. The particle diameters are very close to 1 μm and in some cases the experiments were conducted with submicrometric particles. The material (silica in some cases) has a density of about 2000 kg/m^3 (silica). The main results reported in this work can be summarized as follows:

- for impact velocities in the range 1 m/s–10 m/s, the kinetic energy is typically reduced to one-half for the 1.2 μm and to one-quarter for the 0.5 μm;
- for impact velocities exceeding 10 m/s, the bouncing collisions reduce the kinetic energy by more than one order of magnitude;
- for the 1.2 μm diameter silica spheres, the capture velocity is independent of the target surface tilt angle (0 deg–60 deg);
- electrostatic effects occur during the test and the action of the electrostatic field is observed up to 40 μm from the surface. The same effect can be found in Ref. [12];
- experimental results obtained with irregular shaped particles show a higher capture velocity and, at the same time, a higher SP.

The SP is the one of the most interesting quantities used in this type of study. The SP was evaluated by a statistical approach. It compares the impact that results in sticking with the total amount of impacts. For the SP, the most common threshold limit is equal to 0.5. If more than 50% of the sampled impact results in sticking between the particle and surface, the final results will be sticking or, vice versa, if less than 50% of the sampled impact results in sticking, the final result will be bounce. With this approach, the authors wish to emphasize that the particle impacts are different from each other and, in order to provide a macroscopic evaluation of the results, a statistic/probabilistic approach is the best way.

From the reported literature, it is easy to understand that for the total comprehension of the fouling phenomena it must be known *how* the contaminants hit the blade surface. In this context, the word *how* refers to the impact velocity and the impact angle for each particle. In this paper, for the first time, we will show the kinematic characteristics of the particle impact on the axial compressor blades by means of a CFD numerical simulation.

In literature, some interesting experimental and numerical studies on particle ingestion can be found. In particular, research regarding particle erosion and deposition in gas turbines can be found in Refs. [13] and [14], while for the axial compressor some interesting results can be found in Refs. [15] and [16]. We will focus only on the axial compressor studies. In Ref. [15], the authors performed a study of the erosion effects in an axial compressor stage. The particles have a diameter equal to 165 μm and the results show the particle trajectories also after the first impact. In the case of the second impact, the erosion magnitude is very low due to the low particle kinetic energy. Ghenaiet [16] studied the particle dynamics and erosion of the front compression stage of a turbofan PW-JT8-D17. Particle trajectory simulations used a stochastic Lagrangian tracking code and the sand particle size varies from 0 μm to 1000 μm. The numerical simulations show a different trajectory for the different particle diameter. The larger particles are affected by inertia and centrifugal forces and after the first impact, they do not follow the airflow stream. The smaller particles, $\approx$ 10 μm, tend to follow the flow path closely and are strongly influenced by the flow turbulence, secondary flows, and flow leakage above the blade tip and in due course, induce erosion of the blade tip and shroud. Particles with a diameter less than 10 μm were not taken into account for the erosion analyses, since particles of this size do not carry enough energy to cause erosion.

In the present work, the authors presented a CFD study for the ultrafine powder ingestion (particle size of 0.25 μm–2.00 μm) by an axial compressor rotor, the NASA Rotor 37. These particle sizes can cause fouling, but are too small to cause erosion. The particle ingestion was studied by using a CFD commercial code. In particular, in this second part, the authors, beginning with the results reported in Ref. [6], will show the kinematic characteristics of particle impact on the blade surface. This paper includes the following points:

- a short reference of the numerical model adopted for the continuous and discrete phase (validation and more details can be found in Ref. [6]);
- a short summary of the particle impact zones on the blade surface in order to better understand the following analyses (extensive analyses can be found in Ref. [6]);
- analyses of particle impact velocity and particle impact angle for the pressure side (PS) and SS;
- an analysis of the normal and tangential velocity component in order to define the relative impact kinematic characteristics between blade and particles;
- estimates of the SP up to 1 μm particle diameter in order to define the preferable deposition zones on the blade as a function of the particle diameter.

Numerical Model

Continuum Phase. The reference compressor stage is the NASA Rotor 37 [17]. It is composed of 36 blades but only a single passage vane was modeled. The tip clearance at design speed is 0.356 mm (0.45% of the blade span). All the simulations were performed in a steady multiple frame of reference by using a frozen stage interface. A multiblock hexahedral grid with a total number of 1,131,063 elements was used. The numerical simulations were carried out by means of the commercial CFD code ANSYS FLUENT 13.0 [18]. The standard k-ε turbulence model with a standard wall function was used. The numerical CFD results are in fairly good agreement with the experimental data. The numerical pressure ratio β and the total-to-total efficiency η_{TT} always underestimate the experimental data but in a very consistent way. The deviation in terms of mass flow rate at the choked-flow condition is about 1.87% (all the simulations refer to design speed equal to 17,188 rpm). More details for the numerical domain and validation are given in Ref. [6].

Discrete Phase. In this paper, the solution approach is based on a mathematical model with Eulerian conservation equations in the continuous phase and a Lagrangian frame to simulate a discrete second phase. In this approach, the airflow field is first simulated, and then the trajectories of individual particles are tracked by integrating a force balance equation on the particle. The force balance is comprehensive of inertia, drag, and buoyancy term. In the force balance, there are two contributes due to the shear stress and diffusion called Saffman's lift force and Brownian force but these two contributes become important in very few cases. In this paper, only the Brownian term was neglected. An extensive description of the force balance can be found in Ref. [6].

The dispersion of particles in the fluid phase can be predicted by using a stochastic tracking model. This investigation used the discrete random walk (DRW) model to simulate the stochastic velocity fluctuations in the airflow. The number of trajectories was selected in order to satisfy the statistical independence, since the turbulent dispersion is modeled based on a stochastic process. The inlet/injection surface was made by 1888 uniformly distributed elements and each analysis of three different injections with 1500 trajectories was carried out.

For the particle–wall interaction boundary conditions, the following conditions have been adopted: (i) ideal adherence condition (named *trap*) on the blade surfaces and (ii) nonadherence condition (named *reflect*) on the hub and shroud surfaces. These conditions allow the evaluation of where and how the contaminants encountered the blade surface for the first time, avoiding the introduction of inaccuracies due to the use of bounce models not fully representative of the real conditions. The authors have implemented specific functions and a restitution coefficient for the near-wall particle behavior. The model functions are defined in agreement with Ahlert's [19] model and Forder's [20] coefficients. More details regarding particle–wall interaction can be found in Ref. [6].

The density particle is equal to 2560 kg/m^3 and the variation of the particle diameter, d_p, is in the range of 0.25 μm–2.00 μm, while the Stokes number (calculated at the inlet of the numerical model) is in the range of 0.0010–0.0630. All particles are spherical and nondeformable.

All the analyses refer to injections having particles with the same diameter, the same material, and thus characterized by the same Stokes number. On the other hand, the total flow rate of the discrete phase m_p is linked to the work environment of the compressor and the efficiency of the filtration system. For this reason, a different value of total flow rate of contaminants was imposed at the inlet of the compressor. All injections take place on a previously solved flow field, with the compressor operating at the best efficiency point. All results presented in this paper were obtained from convergent simulations, with a variation of the residues of the motion and turbulent equations close to zero. The injection data are summarized in Table 1 (more details can be found in Ref. [6]).

Previous Results

In this paragraph, the previous results referring to the particle impact on the NASA Rotor 37 blade are summarized. The entire

Table 1 Characteristics of the injections

Case	1	2	3	4	5
Particle diameter, d_p (μm)	0.25	0.50	1.00	1.50	2.00
Stokes number, St	0.0010	0.0039	0.0158	0.0355	0.0630
Total flow rate, m_p (kg/s)	3.51×10^{-6}	2.46×10^{-5}	8.43×10^{-5}	7.59×10^{-5}	4.50×10^{-5}

Table 2 Particle impact distributions

Case	1	2	3	4	5
η_{hit}	2.38	3.18	4.48	7.99	13.76
$\eta_{hit,PS}$	1.66	2.75	4.31	7.87	13.72
$\eta_{hit,SS}$	0.72	0.43	0.17	0.11	0.04
$\eta_{SIDE,PS}$	69.70	86.40	96.20	98.60	99.70
$\eta_{SIDE,SS}$	30.30	13.60	3.80	1.40	0.30

analysis is reported in Ref. [6]. Only a portion of particles injected from the inlet surface of the numerical model has an impact with the blade surface, and due to the imposed surface condition (trap), the contact results in a permanent adherence. For the comparison between the studied cases, two types of percentage were used. The first one is defined as the ratio between the number of particles that hit (and then could stick to) the blade and the total number of injected particles. The second one is defined as the ratio η_{side} between the impacting particles on the PS $\eta_{SIDE,PS}$ or SS $\eta_{SIDE,SS}$ compared to the total number of impacting particles on the blade. In order to provide a useful value of the impacting particles, η_{hit} are also reported for the PS $\eta_{hit,PS}$ and SS $\eta_{hit,SS}$ and refers to the percentage of impacting particles on the PS or SS compared to the total number of injected particles, respectively. All values in Table 2 are reported but an extensive analysis can be found in Ref. [6].

Analyses of the Particle–Blade Interaction

Accretion Rate (AR). The first analysis of the particle–blade interaction refers to the quantity defined as AR which allows the identification of contaminant deposition intensity in terms of kg/m^2 s. The AR, defined on a blade surface, allows the evaluation of the combined effects between the trajectories of the particles and the contaminant total mass flow rate. The AR values are obtained for each run of the respective cases. As mentioned above, each case was repeated for three different runs in order to avoid the problem caused by the statistical resolution of particle tracking. In Table 3, the values of the peak AR* and the values obtained by a weight-area average $\widetilde{\mathrm{AR}}$ for all of the executed runs are reported. From the values of Table 3, it is possible to note that the values obtained for the three runs of each case have the same order of magnitude, confirming the independence of the results from the statistical dispersion. With this evidence, it is possible to define an average value $\overline{\mathrm{AR}}$ of the $\widetilde{\mathrm{AR}}$ for the three runs in each case. With these values, the amount of contaminants that affected the blade surface during the operation can be evaluated. In fact, it is possible to calculate the contaminant mass M_c on the blade surface as

Table 4 Mass contaminant on the blade (kg)

d_p (μm)	Operating time t: 1 h	1 day	2 days	1 week
0.25	0.001	0.022	0.043	0.151
0.50	0.008	0.203	0.404	1.421
1.00	0.453	10.861	21.721	76.025
1.50	0.086	2.054	4.107	14.375
2.00	0.067	1.601	3.203	11.210

$$M_c = \overline{\mathrm{AR}}\, A_b\, t \tag{1}$$

where A_b is the blade surface and t is the operating time. Table 4 summarizes the mass of contaminants on the blade surface for different operation times.

The blade contamination is very noticeable with a very high contaminant mass on the blade surface (up to 76 kg) even after one operation week. These values of the mass deposits are due to the numerical model wall condition on the blade surfaces (trap) that imposes an ideal adhesion for each particle that hits the blade. Hence, the absolute values are not representative of the particle deposition because the sticking phenomena change during the particle deposition due to the different characteristics between the blade surface and the deposited particle layer. Rather, they are representative of the total amount of contaminants which hit the blade.

Impact Velocity

The first analysis is related to the particle impact velocity v_i. The modules of the particle impact velocity are reported in Fig. 1. The velocity values refer to the vector sum of the three velocity components u along the coordinate axes x, y, and z at the impact point on the blade surface. In Fig. 1, the most representative strips are reported: second, sixth, and tenth (12%, 47%, and 83% of the span blade, respectively) divided into PS and SS. Each dot on the graph corresponds to the impacting particle on the blade. From Fig. 1, it can be noticed that

– the impact velocity increases with the height of the blade and this phenomenon is due to the peripheral velocity;
– the lowest impact velocity can be found on the leading edge (LE) and on the trailing edge (TE) of the SS;
– the highest impact velocity can be found on SS, in particular, on the first part of the airfoil chord;
– the effects of flow separation (due to the shock wave) can be clearly seen on the SS. This phenomenon causes the drop of

Table 3 AR values (kg/m^2 s)

	First run		Second run		Third run		Average
d_p (μm)	AR*	$\widetilde{\mathrm{AR}}$	AR*	$\widetilde{\mathrm{AR}}$	AR*	$\widetilde{\mathrm{AR}}$	$\overline{\mathrm{AR}}$
0.25	4.1×10^{-3}	1.1×10^{-5}	1.3×10^{-2}	3.3×10^{-5}	2.1×10^{-2}	5.6×10^{-5}	3.3×10^{-5}
0.50	4.7×10^{-2}	1.1×10^{-4}	1.4×10^{-1}	3.1×10^{-4}	2.4×10^{-1}	5.2×10^{-4}	3.1×10^{-4}
1.00	3.0×10^{0}	1.0×10^{-2}	4.5×10^{0}	1.5×10^{-2}	7.6×10^{0}	2.5×10^{-2}	1.7×10^{-2}
1.50	5.6×10^{-1}	3.1×10^{-3}	4.4×10^{-1}	2.4×10^{-3}	7.4×10^{-1}	4.0×10^{-3}	3.2×10^{-3}
2.00	1.8×10^{-1}	8.3×10^{-4}	5.2×10^{-1}	2.5×10^{-3}	8.5×10^{-1}	4.1×10^{-3}	2.5×10^{-3}

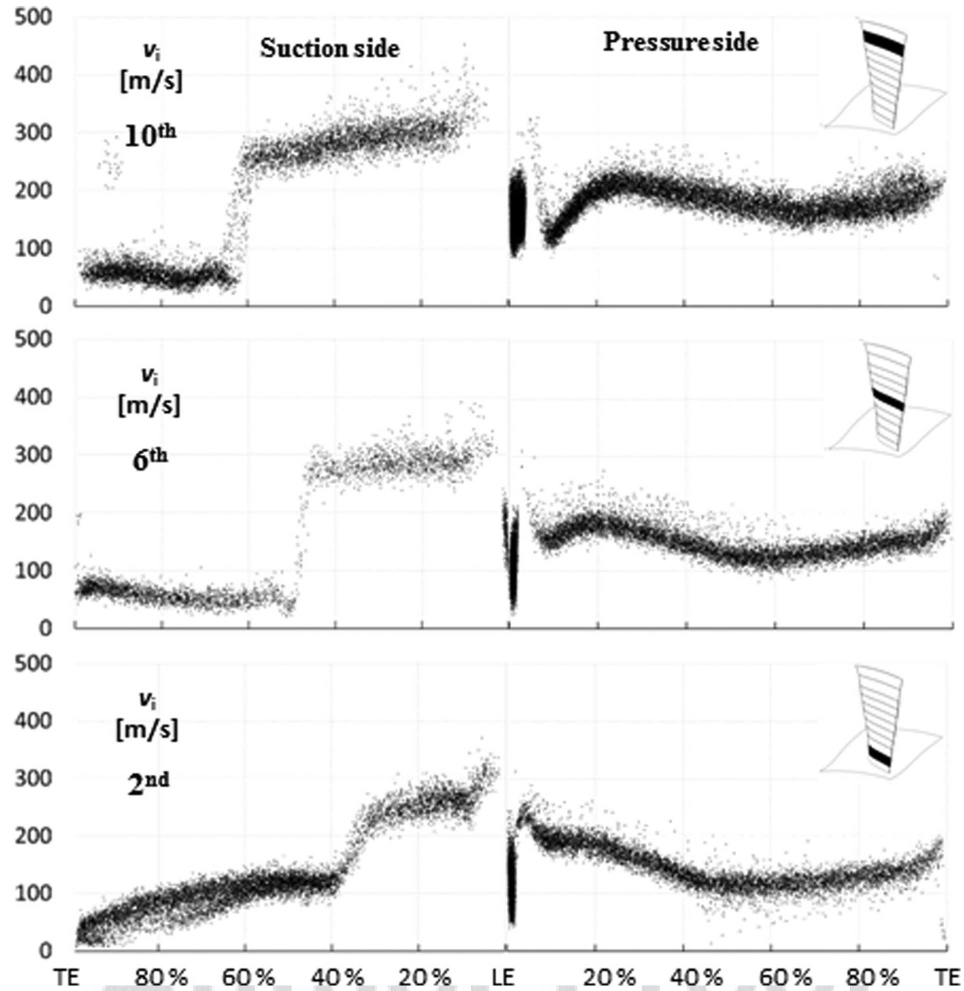

Fig. 1 Impact velocity v_i, second, sixth, tenth strip, case 1

the particle impact velocity and at about 50% of the chord we find the lowest impact velocity;

– on the PS, the velocity trend is very similar for all the strips. On the first part of the chord, the particles reach the peak of impact velocity, while at about the 60% of the airfoil chord the impact velocity reaches a minimum.

The analysis of Fig. 1 shows that the particle impact velocity is very different on the same side of blade. This difference is due to the shape of the blade (e.g., the blade height) and the fluid dynamic phenomena (e.g., flow separation). Another fluid dynamic phenomenon that influenced the particle impact velocity at the top of the blade is the tip leakage vortex due to the blade tip gap. The effect on the particle impact location of this particular phenomenon is clearly investigated in Ref. [6] and in this second part, its effect on particle velocity impact can be seen. As is shown for the SS in Fig. 1, the rear part of the airfoil chord is impacted by particles with a very low impact velocity while for the 11th strip, reported in Fig. 2, this is not quite the case. The rear part of the airfoil chord of the 11th strip is impacted at the same time by particles with very low and very high impact velocity. The particles with the highest impact velocity are the particles dragged by the tip leakage vortex from the PS to the SS.

In this specific case, the wall condition imposed on the blade (trap) determines a smaller amount of particles that are dragged from the PS to the SS. Under real conditions, some particles bounce off the PS and could reach the other side of the blade through the tip gap. This effect plays a key role in the erosion problem not considered in this work due to the small particle sizes. In fact, the erosion phenomena require a particle diameter larger than 10 μm as reported by Hamed et al. [13], Ghenaiet [16], and Kurz and Brun [21].

Impact Angle. As can be seen from the previous analyses, the particle impact velocity changes from the hub to the shroud, from the PS to the SS and along the airfoil chord. However, the impact velocity v_i is not the only parameter needed to determine particle adhesion on the blade surface. As mentioned above, particle adhesion is due to a combination of a number of effects, but the most important parameters are the normal v_n and tangential v_t velocity

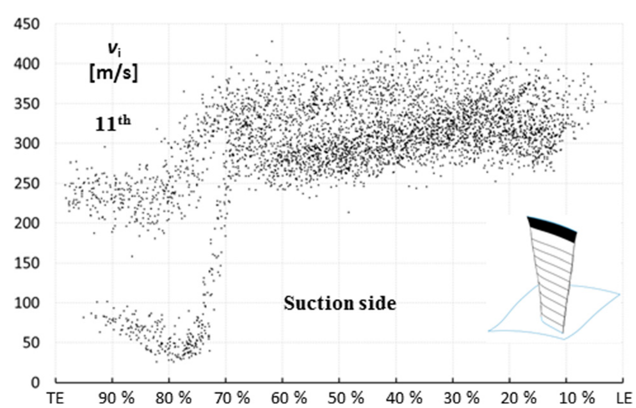

Fig. 2 Impact velocity v_i, 11th strip SS, case 1

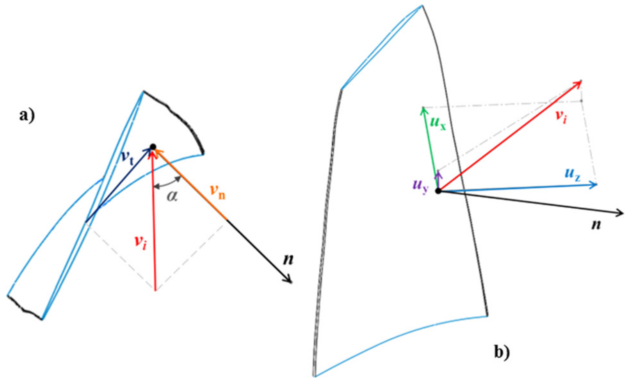

Fig. 3 Particle vectors velocity: (*a*) normal and tangential impact velocity and (*b*) impact velocity

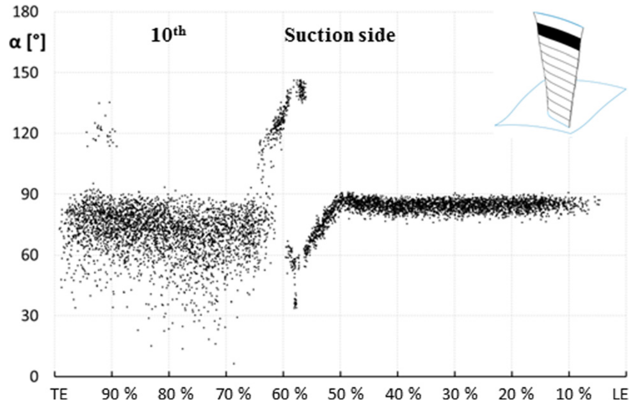

Fig. 5 Impact angle α, tenth strip, SS, case 1

components. In this paragraph, we analyze the particle impact angle in order to better understand the particle kinematic impact.

The impact velocity was obtained by a vector sum of the three velocity components u_x, u_y, and u_z along the axes x, y, and z, respectively (Fig. 3(*b*)). The impact velocity was decomposed with respect to the normal (v_n) and tangential (v_t) direction (Fig. 3(*a*)). Thus, the impact angle α is the angle between the surface normal vector n and the impact velocity vector v_i.

In Figs. 4 and 5, the particle impact angle for the PS of the sixth strip and for the SS of the tenth strip (case 1) are reported. We find in Figs. 4 and 5 that in some instances the impact angle is higher than 90 deg. This is due to (i) the surface local curvature (e.g., at the LE and on the TE) and (ii) surface reconstruction approximation during the particle impact postprocess. A deviation can arise from the fact that the surface is reconstructed by interpolating points on the mesh elements in the neighborhood of the point of impact. The approximation introduced by this procedure is considered acceptable by the authors, allowing for a confidence band of ± 5 deg for all the results shown in this paper.

Figures 4 and 5 illustrate the following observations:

– the impact angle at the LE (Fig. 4(*a*)) assumes different values from 30 deg to 120 deg;

– on the PS (Fig. 4(*a*)), the particle impact angle is very close to 90 deg (i.e., the particles are tangential to the blade surface) almost everywhere on the airfoil. A particular area can be noticed in the middle of the chord where the particle impact angle reaches 120 deg. This fact is consistent with Fig. 5(*b*) where the representation of the PS curvature is reported. The blue zone refers to a lower curvature, while the red zone refers to higher curvature. The local variation of the impact angle (gray box) corresponds to the local variation of the surface curvature (gray circle). Thus, it is clearly shown that the local curvature of the airfoil (e.g., dimples, surface damage, etc.) changes the particle impact angle in a significant way and, more generally, the local shape of the blade changes the particle deposition. A different impact angle can determine whether the particle sticks or slips and thus, the actual shape of the blade surface would determine the magnitude and the rate of the fouling. These findings represent a useful guide for blade surface treatment and control during the manufacturing and maintenance process. The same phenomenon can be noticed for all the strips;

– for the SS, there is also a variation of the particle impact angle in the middle of the chord due to the airfoil curvature. However, it is less noticeable than on the PS;

– on the SS, the particle impact angle is lower than the PS and this implies that the particle hits the surface with a value of normal velocity higher than the tangential velocity. This is noticeable in the last part of the chord where the flow is separated from the blade.

Areas characterized at the same time by very high tangential velocity and very low normal velocity (impact angle close to 90 deg) should not be subject to particle deposition because in this case the particles tend to slip on the blade surface. However, in the other areas with a lower impact angle, the normal velocity promotes particle sticking (e.g., in the case of ductile particles). Similar evaluations can be made for cases in which the blade surface is contaminated by water, oil, or grease and in the case of viscous particles (e.g., oils and grease) that should stick to the blade surface more easily because of the high normal velocity. A study on particle sticking by liquid materials can be found in Ref. [22] in which the authors show the coefficient of restitution trend for molten granulate. For this material, the results show a lower bounce capability at high impact velocities.

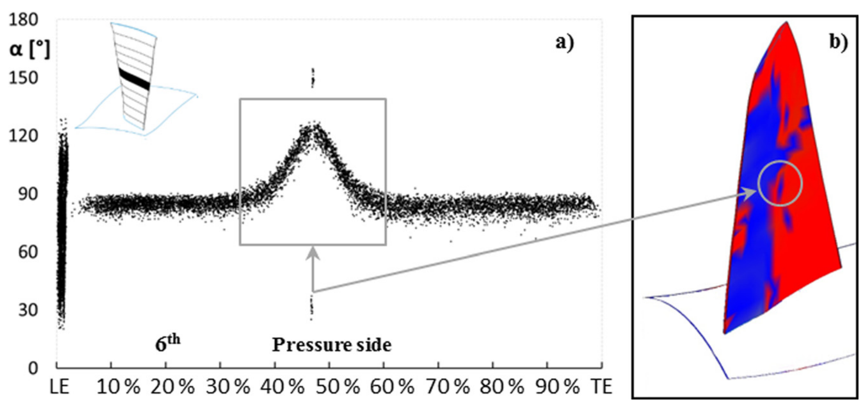

Fig. 4 (*a*) Impact angle α, sixth strip, PS, case 1 and (*b*) contour plot of the PS curvature

However, these preliminary considerations must also be related to the material properties (particles and surface) and to the surface roughness (high or low). The particle slip is related to the surface roughness. Greater roughness causes more slip resistance and therefore easier adhesion or easier breaking away of particles [23].

As shown in the first paragraphs, the study of particle adhesion on a surface comprises a large number of aspects and probabilistic analyses are often used due to the unique nature of each contact. In this paper, the authors provide a quantitative analysis of particle adhesion by using the experimental results found in Ref. [11] in which particle velocity and materials are among the most similar to the particles causing fouling phenomena.

SP. The SP analysis is closely related to the experimental results provided by Poppe et al. [11]. The SP defined in Ref. [11] was calculated for each normal impact velocity v_n by sliding averaging in groups. The groups consisted of 11 collision events for the smallest and largest velocities, respectively, and of up to 71 collision events for the intermediate velocities, thus accounting for the uneven velocity distribution of the impacts. The upper and lower standard deviations (1σ) for the SP are reported in Figs. 6 and 7 (black continuous lines). The trends refer to irregular grains of silicon carbide ($\rho_p \approx 3000\,\mathrm{kg/m^3}$, $E \approx 410\,\mathrm{GPa}$, and hardness $\approx 2800\,\mathrm{kg/mm^2}$) with an average diameter equal to 0.37 μm and 0.64 μm that impacts a dry, polished silica surface. In Figs. 6 and 7, SEM images of a silicon carbide sample are also reported. The SP among the 11 slowest and the 11 fastest collisions is separately given as a constant value in the corresponding velocity interval (reported with a linear segment in Figs. 6 and 7). The capture velocity is the velocity where the 1σ limits of the SP are 0.5. Such a definition results in a physically meaningful quantity only if the SP behaves similarly to a step function. More details on materials and experimental results can be found in Ref. [11].

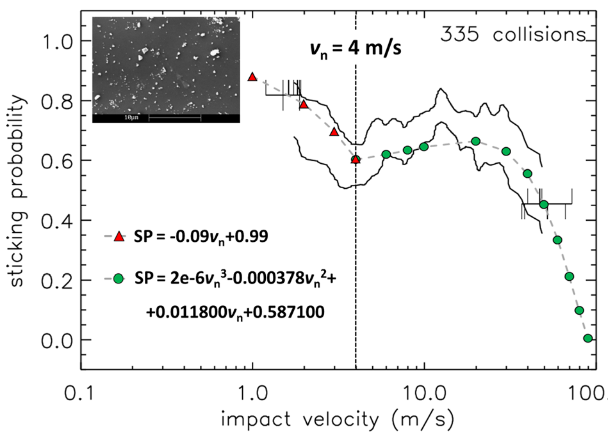

Fig. 6 SP versus normal impact velocity v_n of silicon carbide particles, 0.37 μm on silica target [11], and trend of adopted equations superimposed

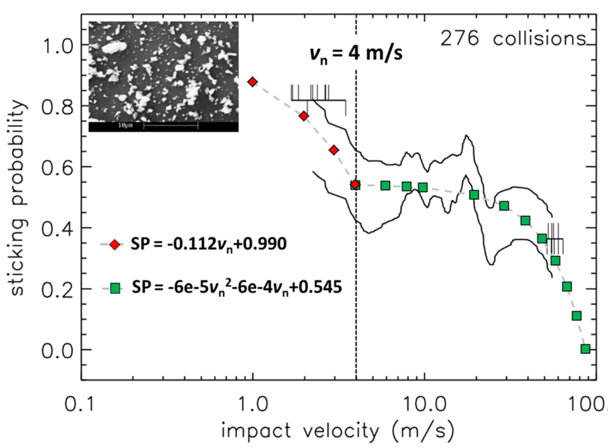

Fig. 7 SP versus normal impact velocity v_n of silicon carbide particles, 0.64 μm on silica target [11], and trend of adopted equations superimposed

With the experimental SP trend reported in Figs. 6 and 7, it is possible to define representative trends for the correlation between the normal impact velocity v_n and the SP. For the smaller silicon carbide particles (0.37 μm) reported in Fig. 6, the trend can be represented by two equations. The first one refers to the lower normal impact velocity (<4 m/s)

$$S_p = -0.09\,v_n + 0.99 \tag{2}$$

and the second one refers to normal impact velocity in the range of 4 m/s–90 m/s

$$S_p = 2 \times 10^{-6}\,v_n^3 - 0.000378\,v_n^2 + 0.011800\,v_n + 0.587100 \tag{3}$$

The results of Eqs. (2) and (3) are reported in Fig. 6, with the experimental results obtained by Poppe et al. [11] superimposed. As can be noticed from Eq. (2), in the case of the normal impact velocity equal to 0 m/s, the SP is equal to 0.99.

In the same way, for the larger silicon carbide (0.64 μm) reported in Fig. 7, the trend can be represented by two equations. The first one refers to the lower normal impact velocity (<4 m/s)

$$S_p = -0.112\,v_n + 0.990 \tag{4}$$

and the second one refers to normal impact velocity in the range of 4 m/s–90 m/s

$$S_p = -6 \times 10^{-5}\,v_n^2 - 6e - 4\,v_n + 0.545 \tag{5}$$

Again, the results of Eqs. (4) and (5) are reported in Fig. 7, with the experimental results obtained by Poppe et al. [11] superimposed. The threshold normal velocity (equal to 4 m/s) and the degree of the polynomials were chosen in order to better describe the experimental trend results.

With the definition of the SP (Eqs. (3) and (5)), for cases 1 and 2, the SP = 0.5 is in correspondence to a normal impact velocity v_n equal to 48.35 m/s. However, for case 3, the SP = 0.5 is in correspondence to a normal impact velocity v_n equal to 22.85 m/s. Thus, the smaller particles have a wider range of normal impact velocity for which particle impact with the blade surface becomes (with a high probability) a permanent adhesion.

Equations (2)–(5) are used to calculate the SP for each particle stuck to the blade surface by using the normal impact velocity. The particle characteristics used in Ref. [11] are quite different compared to the classic particle characteristics involved in fouling phenomena. In particular, the silicon carbide particles [11] have a very high level of hardness and this implies that the rebound properties could be different from those found in the real fouling applications.

In Fig. 8, the SP for the sixth strip (case 1) is reported. Each dot on the graph represents a particle that hit the blade surface with a normal impact velocity less than 90 m/s. Only the particles with a normal velocity component toward the surface are taken into account. This procedure allows the identification of the dangerous particle (that will be able to stick) with respect to fouling phenomenon only. Figure 8 illustrates that

– the SS is completely covered by particles that have a SP of about 0.7;
– the PS shows an area, in the middle of the airfoil chord, in which the particles have a SP equal to zero. This effect is due

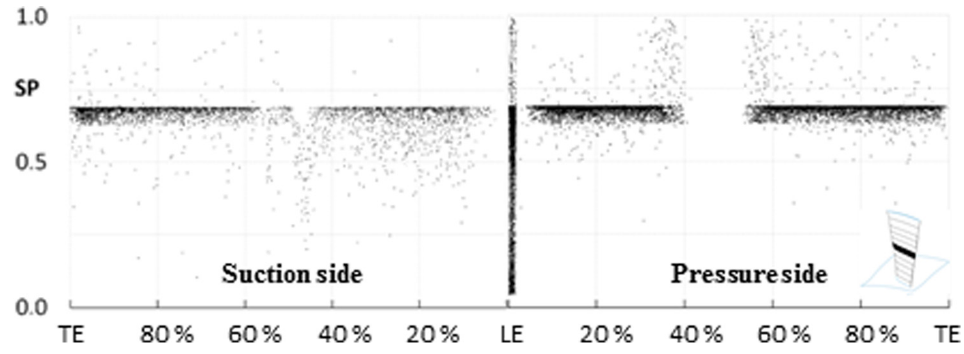

Fig. 8 SP, sixth strip, case 1

to the airfoil shape as highlighted in Fig. 4. For the other regions in the PS, the SP is comparable with the SP on the SS, and in some cases reaches the unit;
- on the LE, there are very dispersed values of SP, probably due to the wide range of the impact angle as can be seen in Fig. 4.

The other strips show similar features. As mentioned above, the SP defined in Ref. [11] only considers the normal impact velocity. However, in this application, particular attention must be paid to the tangential impact velocity. In fact, as can be seen in Fig. 9 for the sixth strip, the magnitude of the tangential impact velocity is not negligible. The tangential impact velocity can reach 250 m/s or 400 m/s in the PS and SS, respectively. These very high values may diminish the SP and transform the adhesion-impact in to the slip-impact. Conversely, it can be noted that in the separation zone on SS, where the SP is equal to 0.7, the tangential impact velocity is much smaller, thus limiting the possibility of slip between the particle and blade surface. Regarding this aspect, some field data can be found in Ref. [24], where the authors highlighted the higher deposition rate where the shear stress between air and blade surface is lower. This confirms the results obtained in this work by linking together the SP data and the impact dynamic characteristics.

Unfortunately, specific studies on the interaction between normal impact velocity, tangential impact velocity, and surface roughness are not available in literature. In addition, specific studies on the variation of the SP due to the presence of a third material at the interface between surface and particle are not available in literature. Poppe et al. [11] pointed out that the presence of hydrophobic silane coating did not change the collisional behavior with respect to another test in which the surface was only cleaned with alcohol and subsequently dried with pressurized air.

Generally, in the actual compressors, the presence of a third substance (such as oil and grease) on the blade surface could increase the SP of the particle, but, at the moment, there are no specific studies that allow the quantification of this effect.

In Table 5, all the impact characteristics are reported for cases 1, 2, and 3 that are considered by the authors the most interesting cases from a fouling point of view.

The particles are subdivided by using normal impact velocity criteria. In particular, the following three categories are defined:

- the particles that move away from the surface (called harmless);
- the particles that have a normal impact velocity less than 90 m/s and for which it can be possible to define an SP by using Eqs. (2)–(5);
- the particles that have an impact normal velocity higher than 90 m/s and for which the SP is assumed equal to zero.

Special attention must be paid to the last category, characterized by an impact normal velocity higher than 90 m/s and an SP equal to zero. These particles possess high kinetic energy that decreases by an order of magnitude during the first impact as reported in Ref. [11]. This phenomenon implies that these particles will not be able to stick during the first contact but instead, it will most likely be during the second one. In fact, the decrease in kinetic energy is strongly related to the decrease in velocity and, consequently, an increase of SP. A similar effect can also be found in turbomachinery applications. In Ref. [15], the authors have described the poor erosion capacity shown by the particles during the second contact with the blade caused by a low level of kinetic energy that corresponds to that observed in Ref. [11]. If this phenomenon is not important from an erosion point of view (due to the particle diameter lower than 10 μm), for the fouling problems, a low particle kinetic energy during impact with the blade leads to a high SP.

Table 5 shows for all categories listed above: (i) the absolute number of particles N that have impacted on that side (PS or SS) and on that band (1st–11th), (ii) the ratio n_{SIDE} between the absolute number N and the total number of particles that impacted on that side of the blade, and (iii) the ratio n_{hit} between the absolute number N and the total number of injected particles. Thus, the ratio n defines the kinematic characteristics distribution on one

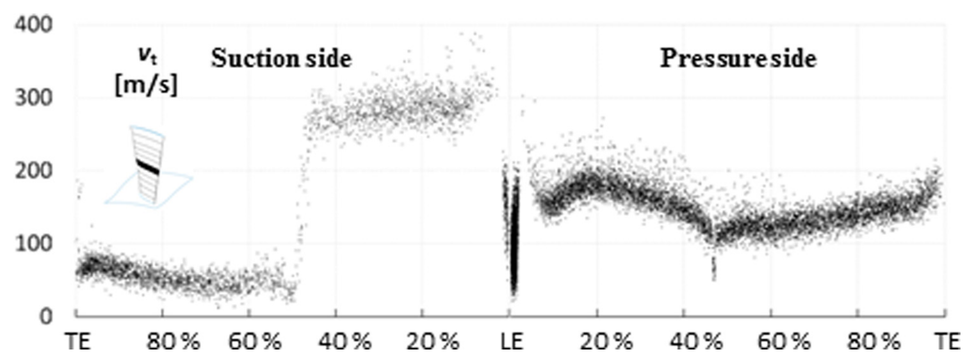

Fig. 9 Tangential velocity v_t, sixth strip, case 1

J_ID: TURB DOI: 10.1115/1.4028296 Date: 21-August-14 Stage: Page: 9 Total Pages: 13

Table 5 Particle–blade interaction

		Case 1 ($d_p = 0.25\ \mu m$)						Case 2 ($d_p = 0.50\ \mu m$)						Case 3 ($d_p = 1.00\ \mu m$)					
		PS			SS			PS			SS			PS			SS		
		N	n_{SIDE} (%)	n_{hit} (%)	N	n_{SIDE} (%)	n_{hit} (%)	N	n_{SIDE} (%)	n_{hit} (%)	N	n_{SIDE} (%)	n_{hit} (%)	N	n_{SIDE} (%)	n_{hit} (%)	N	n_{SIDE} (%)	n_{hit} (%)
11th	Harmless	8004	5.69	0.09	1333	2.18	0.02	17,091	7.32	0.20	423	1.15	0.00	29,258	8.00	0.35	118	0.81	0.00
	$0 < v_n \le 90$ m/s	4392	3.12	0.05	2678	4.38	0.03	3600	1.54	0.04	1074	2.92	0.01	7259	1.99	0.09	96	0.66	0.00
	$v_n > 90$ m/s	283	0.20	0.00	328	0.54	0.00	290	0.12	0.00	102	0.28	0.00	357	0.10	0.00	13	0.09	0.00
	$SP \ge 0.5$	4045	2.88	0.05	1717	2.81	0.02	3354	1.44	0.04	828	2.25	0.01	4337	1.19	0.05	44	0.30	0.00
Tenth	Harmless	5606	3.99	0.07	335	0.55	0.00	11,646	4.99	0.14	157	0.43	0.00	13,168	3.60	0.16	84	0.58	0.00
	$0 < v_n \le 90$ m/s	15,102	10.74	0.18	6385	10.44	0.08	21,913	9.39	0.26	3278	8.92	0.04	33,297	9.11	0.39	78	0.54	0.00
	$v_n > 90$ m/s	669	0.48	0.01	191	0.31	0.00	83	0.04	0.00	97	0.26	0.00	146	0.04	0.00	1	0.01	0.00
	$SP \ge 0.5$	11,943	8.49	0.14	5951	9.73	0.07	18,183	7.79	0.21	3065	8.34	0.04	22,125	6.05	0.26	64	0.44	0.00
Nineth	Harmless	2249	1.60	0.03	71	0.12	0.00	1851	0.79	0.02	50	0.14	0.00	1620	0.44	0.02	4	0.03	0.00
	$0 < v_n \le 90$ m/s	11,079	7.88	0.13	5011	8.20	0.06	18,876	8.09	0.22	2849	7.75	0.03	25,338	6.93	0.30	175	1.20	0.00
	$v_n > 90$ m/s	1216	0.86	0.01	113	0.18	0.00	1784	0.76	0.02	52	0.14	0.00	3755	1.03	0.04	4	0.03	0.00
	$SP \ge 0.5$	9049	6.43	0.11	4729	7.73	0.06	12,442	5.33	0.15	2634	7.17	0.03	14,819	4.05	0.17	103	0.71	0.00
Eighth	Harmless	2159	1.53	0.03	385	0.63	0.00	1996	0.85	0.02	90	0.24	0.00	2544	0.70	0.03	0	0.00	0.00
	$0 < v_n \le 90$ m/s	13,206	9.39	0.16	6724	11.00	0.08	24,456	10.48	0.29	4011	10.91	0.05	35,757	9.78	0.42	207	1.42	0.00
	$v_n > 90$ m/s	1403	1.00	0.02	35	0.06	0.00	3462	1.48	0.04	11	0.03	0.00	9268	2.54	0.11	0	0.00	0.00
	$SP \ge 0.5$	11,711	8.33	0.14	6321	10.34	0.07	13,522	5.79	0.16	3704	10.08	0.04	18,874	5.16	0.22	126	0.87	0.00
Seventh	Harmless	2974	2.11	0.04	319	0.52	0.00	3203	1.37	0.04	63	0.17	0.00	5041	1.38	0.06	8	0.05	0.00
	$0 < v_n \le 90$ m/s	13,162	9.36	0.16	4969	8.13	0.06	24,158	10.35	0.28	2159	5.87	0.03	43,160	11.81	0.51	65	0.45	0.00
	$v_n > 90$ m/s	1032	0.73	0.01	1	0.00	0.00	3440	1.47	0.04	5	0.01	0.00	9057	2.48	0.11	1	0.01	0.00
	$SP \ge 0.5$	12,071	8.58	0.14	4749	7.77	0.06	17,038	7.30	0.20	2001	5.44	0.02	26,929	7.37	0.32	36	0.25	0.00
Sixth	Harmless	2785	1.98	0.03	381	0.62	0.00	2087	0.89	0.02	15	0.04	0.00	3275	0.90	0.04	0	0.00	0.00
	$0 < v_n \le 90$ m/s	9623	6.84	0.11	3184	5.21	0.04	11,885	5.09	0.14	845	2.30	0.01	18,351	5.02	0.22	1	0.01	0.00
	$v_n > 90$ m/s	539	0.38	0.01	1	0.00	0.00	3000	1.29	0.04	1	0.00	0.00	1207	0.33	0.01	0	0.00	0.00
	$SP \ge 0.5$	8711	6.19	0.10	3063	5.01	0.04	8282	3.55	0.10	810	2.20	0.01	14,195	3.88	0.17	1	0.01	0.00
Fifth	Harmless	1967	1.40	0.02	65	0.11	0.00	665	0.28	0.01	21	0.06	0.00	219	0.06	0.00	0	0.00	0.00
	$0 < v_n \le 90$ m/s	4646	3.30	0.05	4785	7.83	0.06	4649	1.99	0.05	1718	4.67	0.02	1131	0.31	0.01	7	0.05	0.00
	$v_n > 90$ m/s	350	0.25	0.00	0	0.00	0.00	1504	0.64	0.02	2	0.01	0.00	999	0.27	0.01	0	0.00	0.00
	$SP \ge 0.5$	4127	2.93	0.05	4624	7.56	0.05	2192	0.94	0.03	1642	4.47	0.02	968	0.26	0.01	5	0.03	0.00
Fourth	Harmless	5202	3.70	0.06	115	0.19	0.00	5787	2.48	0.07	33	0.09	0.00	1823	0.50	0.02	0	0.00	0.00
	$0 < v_n \le 90$ m/s	8021	5.70	0.09	6057	9.91	0.07	15,357	6.58	0.18	1938	5.27	0.02	17,564	4.81	0.21	222	1.52	0.00
	$v_n > 90$ m/s	254	0.18	0.00	12	0.02	0.00	553	0.24	0.01	22	0.06	0.00	723	0.20	0.01	0	0.00	0.00
	$SP \ge 0.5$	7411	5.27	0.09	5393	8.82	0.06	11,720	5.02	0.14	1722	4.68	0.02	3321	0.91	0.04	22	0.15	0.00
Third	Harmless	4840	3.44	0.06	311	0.51	0.00	7866	3.37	0.09	576	1.57	0.01	6359	1.74	0.08	46	0.32	0.00
	$0 < v_n \le 90$ m/s	4205	2.99	0.05	7074	11.57	0.08	8848	3.79	0.10	2664	7.25	0.03	24,561	6.72	0.29	1416	9.73	0.02
	$v_n > 90$ m/s	526	0.37	0.01	123	0.20	0.00	4149	1.78	0.05	39	0.11	0.00	3112	0.85	0.04	0	0.00	0.00
	$SP \ge 0.5$	3731	2.65	0.04	5940	9.71	0.07	6281	2.69	0.07	2510	6.83	0.03	10,785	2.95	0.13	1326	9.11	0.02
Second	Harmless	6703	4.77	0.08	1372	2.24	0.02	8021	3.44	0.09	5601	15.24	0.07	18,922	5.18	0.22	1774	12.19	0.02
	$0 < v_n \le 90$ m/s	3350	2.38	0.04	6497	10.63	0.08	7879	3.37	0.09	5557	15.12	0.07	13,813	3.78	0.16	2322	15.95	0.03
	$v_n > 90$ m/s	669	0.48	0.01	656	1.07	0.01	3524	1.51	0.04	1409	3.83	0.02	10,017	2.74	0.12	5217	35.84	0.06
	$SP \ge 0.5$	2130	1.51	0.03	3632	5.94	0.04	4166	1.78	0.05	2133	5.80	0.03	1567	0.43	0.02	692	4.75	0.01

Table 5. Continued

		Case 1 ($d_p = 0.25\,\mu$m)						Case 2 ($d_p = 0.50\,\mu$m)						Case 3 ($d_p = 1.00\,\mu$m)					
		PS			SS			PS			SS			PS			SS		
		N	n_{SIDE} (%)	n_{hit} (%)	N	n_{SIDE} (%)	n_{hit} (%)	N	n_{SIDE} (%)	n_{hit} (%)	N	n_{SIDE} (%)	n_{hit} (%)	N	n_{SIDE} (%)	n_{hit} (%)	N	n_{SIDE} (%)	n_{hit} (%)
First	Harmless	3133	2.23	0.04	250	0.41	0.00	6765	2.90	0.08	1339	3.64	0.02	13,741	3.76	0.16	120	0.82	0.00
	$0 < v_n \leq 90$ m/s	1170	0.83	0.01	1385	2.27	0.02	2240	0.96	0.03	560	1.52	0.01	4753	1.30	0.06	2578	17.71	0.03
	$v_n > 90$ m/s	148	0.11	0.00	0	0.00	0.00	834	0.36	0.01	0	0.00	0.00	5924	1.62	0.07	1	0.01	0.00
	SP $\geq$ 0.5	712	0.51	0.01	1345	2.20	0.02	691	0.30	0.01	508	1.38	0.01	566	0.15	0.01	2227	15.30	0.03
Side	Harmless	45,622	32.43	0.54	4937	8.07	0.06	66,978	28.69	0.79	8368	22.76	0.10	95,970	26.26	1.13	2154	14.80	0.03
	$0 < v_n \leq 90$ m/s	87,956	62.53	1.04	54,749	89.54	0.65	14,3861	61.62	1.70	26,653	72.50	0.31	22,4984	61.55	2.65	7167	49.23	0.08
	$v_n > 90$ m/s	7089	5.04	0.08	1460	2.39	0.02	22,623	9.69	0.27	1740	4.73	0.02	44,565	12.19	0.53	5237	35.97	0.06
	SP $\geq$ 0.5	75,641	53.77	0.89	47,464	77.62	0.56	97,871	41.92	1.15	21,557	58.64	0.25	11,8486	32.42	1.40	4646	31.91	0.05

side of the blade for all the particles upon the impact and the ratio n_{hit} shows a global overview, in line with the fouling susceptibility criteria that consists of the ratio between the number of stuck particles and the total number of particles injected in the flow path.

In Table 5, N, n_{SIDE}, and n_{hit} related to the particles characterized by an SP equal to or greater than 0.5 are also reported. Finally, the rows grouped by the name *side* contain the sum of the values reported for each strip. With this global overview, it is possible to highlight the different behavior of particle deposition on the blade surface, in particular:

– the percentages of the particles with $v_n > 90$ m/s are higher for the strips close to the hub in the SS, while in PS this value is higher for the strips close to the blade tip;
– the comparison between cases 1 and 2 shows a different value of the SP > 0.5 between the PS and SS along the blade span. In fact, for the strip close to the hub (second), the particle percentage on SS of the SP > 0.5 is higher than the PS, while at midspan (sixth and seventh), the PS percentage is higher than the SS. At blade tip (11th), the two values are quite similar.

With the spanwise subdivision of the results shown in Table 5, we can highlight the difference in terms of particle–blade interaction behavior between the SS and PS.

Thanks to the sum of the values N, n_{SIDE}, and n_{hit} for the two sides of the blade, further analysis regarding particle–blade interaction is possible.

Figure 10 shows two bar charts relative to the sum of values for the ratio n_{SIDE}, reported for each strip, and indicated with the name n_{SIDE}. On the SS, the percentage of particles with SP > 0.5 is greater than the PS for all cases even if, for case 3, the phenomenon is much less obvious. This result shows how on the SS there are some fluid dynamic conditions that make it more sensitive to particle sticking. On the SS, there are fewer particles than the PS but these particles have a higher sticking capacity. From the compressor performance point of view, the sensitivity to fouling of the SS appears to be greater than the PS [25], thus a greater particle tendency to stick to the SS is an important result and focuses attention not only on the quantity of ingested contaminants but also to the fluid dynamic phenomena that characterize the flow around the blade. On the SS, case 1 is the most severe from a fouling point of view. The particles arrive with a normal impact velocity that makes it extremely effective in sticking to the blade surface. The percentage of particles with an SP > 0.5 reaches almost 90%. On the PS, the differences of the particle impact kinematics are less evident between the cases and all the percentages are quite similar to each other even if case 3 uses a particle diameter four times higher than case 1. The PS, for all cases, shows a higher percentage for the *harmless* particle category. This effect is directly related to the fact that in PS the separation that afflicts the SS does not take place. For the PS and SS, it can be seen that the particle percentage of the $v_n > 90$ m/s category increases with the increase of the particle diameter and the SP decreases as the diameter increases. This phenomenon is the precursor of the erosive effects that are produced by the particles with a diameter greater than 10 μm, as reported in Ref. [16]. In fact, the normal impact velocity increases with the increase of the particle diameter and, in the same way, the particles become less able to stick, although the impact is more dangerous for the blade surface. The final analysis is related to the particles that have the SP > 0.5. In particular, in Fig. 11, the trend of the ratio $n_{hit,SP>0.5}$ (black continuous line) for the particles with SP > 0.5 superimposed with the trend of the η_{hit} (grey dotted line) is reported. The two trends refer to both sides of the blade (PS and SS).

As mentioned above, η_{hit} represents the fouling susceptibility and its values represent a key result for gas turbine operators.

As can be seen from Fig. 11, for the PS, the trend of $n_{hit,PS,SP>0.5}$ does not follow the trend of $\eta_{hit,PS}$ unlike the trends reported for the SS. For the PS, the number of stuck particles is quite independent to the total number of particles that hit the blade and the $n_{hit,PS,SP<0.5}$ remains almost the same for the three

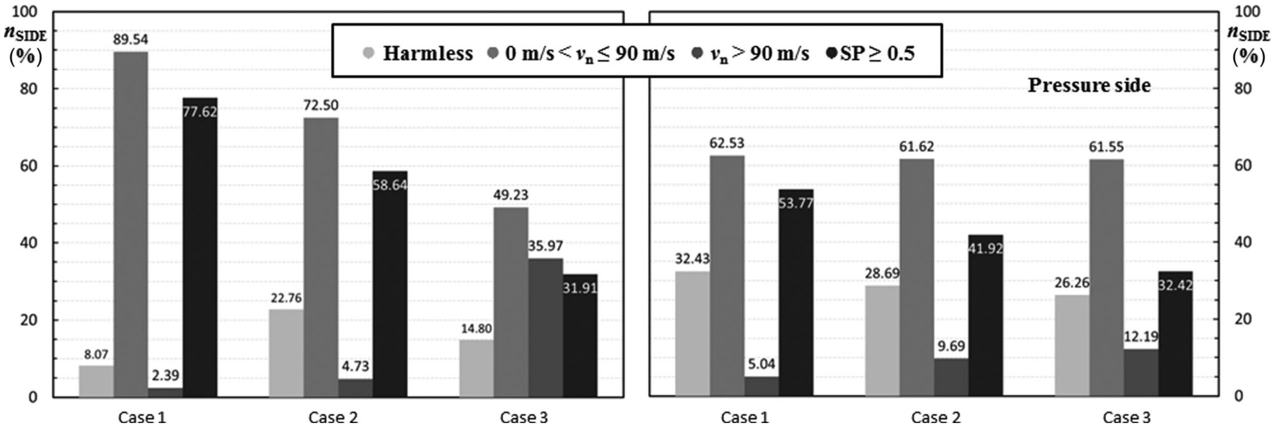

Fig. 10 Ratio n_{SIDE} for the SS and PS of cases 1, 2, and 3

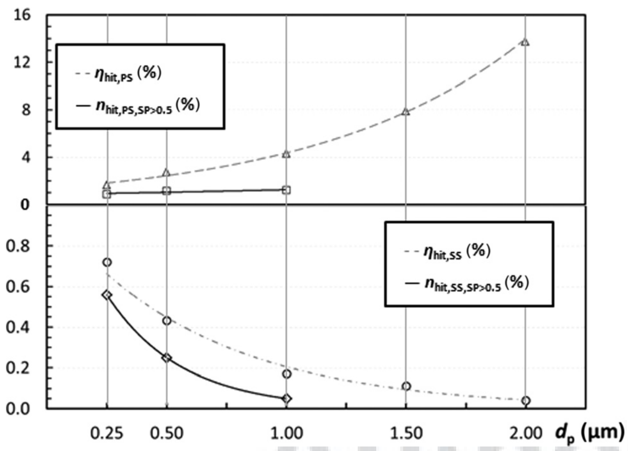

Fig. 11 Trends of the ratio $n_{hit,SP>0.5}$ and η_{hit} superimposed

considered cases. In this case, the higher particles produce more fouling effects due to their higher diameter and thus the higher mass. For the SS, the ratio $n_{hit,SS,SP>0.5}$ shows a very high percentage of particles able to stick for the smallest diameters compared to the total number of particles that hit the SS.

Considering the different effect of the SS and PS deposits on axial compressor performance drop [25], some general guidelines for proper management of the power plant can be described as follows:

– as reported in Ref. [25], the deposits on the SS have the highest influence on the axial compressor performance drop. Therefore, the filtration system must be designed to remove the smaller particles (up to 0.5 μm) from the airflow stream because the bigger particles have a smaller SP and are not able to reach the SS due to their inertia;
– as reported in Ref. [25], the deposits on the PS have the lowest influence on the axial compressor performance drop. Therefore, the bigger particles that could stick on the PS do not determine a great performance drop and these deposits could be removed by proper periodic washing operations.

Conclusions

In this paper, an extended study on microparticle adhesion on the axial compressor blade surface was carried out. The microparticles dragged by the airflow through the air filtration systems are responsible for compressor fouling if they come into contact with the compressor airfoils and stick there.

The kinematic characteristics for the impacting particles are obtained by a numerical model validated by data from literature and are used in order to describe for the first time how the sub micro-sizes particles hit the blade surface. Special attention was given to the particle–blade interaction in terms of impact velocity and impact angle.

Thanks to experimental data reported in literature and the knowledge of the impact velocity component, it has been possible to highlight which blade areas are more affected by particle deposition and their sensitivity to particle diameters and fluid dynamic phenomena.

The key results can be summarized as follows:

– the particle impact velocity depends on several factors: shape of the blade (e.g., the blade height and local airfoil curvature), design characteristics (e.g., tip gap), and fluid dynamic phenomena (e.g., flow separation and tip leakage vortex);
– on the PS, the particle impact angle is very close to 90 deg in almost all of the airfoil extension;
– on the SS, the particle impact angle is lower than the PS due to the separation phenomena. This fact implies that particles hit the surface with a value of normal velocity higher than tangential velocity;
– thanks to the experimental results reported in literature regarding SP, it was possible to define two representative trends for the correlation between normal impact velocity and SP;
– on the SS, the smallest particles are the most numerous from a fouling point of view due to the high total number of particles characterized by a SP greater than 0.5.

Regarding the management of gas turbine installations, the results of this study highlight the advantage of installing air filtration systems that can remove small and very small particles from the air stream. This would allow the use of effective online washing using larger droplets that typically would only hit and clean the PS of the blade.

The CFD numerical simulations link the design characteristic of the machine and the fluid dynamic phenomena. As shown in this work, these two items determine the particle deposition on the blade surface and thus the fouling phenomena. Future studies would have to analyze the behavior of a subsonic stage where the fluid dynamic phenomena are quite different compared to a transonic stage.

An increase in the knowledge of fouling through the use of numerical codes may therefore constitute a decisive element for better planning of maintenance of turbomachinery. In this sense, studies (experimental and numerical) dedicated to the interaction between the particles responsible for fouling (in terms of size and material) with blade surfaces are fundamental to allow for better simulations with numerical codes.

Nomenclature

A = area
d = diameter

E = Young module
k = turbulent kinetic energy
m = mass flow rate
M = mass
n = ratio
N = total number (referred to particles)
r = radius
St = Stokes number
t = operation time
u = velocity component
U = averaged velocity
v = velocity
X = particle concentration (blade)
x, y, z = axis coordinate
α = impact angle
β = compression ratio
ε = dissipation rate of turbulent kinetic energy
η = efficiency
μ = dynamic viscosity
ρ = density
σ = standard deviation

Subscripts and Superscripts

b = blade
c = contaminant
h = hydraulic
hit = hit (referred to blade, side, and slice)
i = impact
n = normal direction
p = particle
SIDE = side (referred to the blade division)
STRIP = strip (referred to spanwise division)
t = tangential direction
TT = total-to-total
x, y, z = axis coordinate
1 = inlet
– = average
∼ = weighted-area average
* = peak

Acronyms

AR = accretion rate
CFD = computational fluid dynamics
DRW = discrete random walk
FDS = flux-difference splitting
LE = leading edge
PS = pressure side
SEM = scanning electron microscope
SP = sticking probability
SS = suction side
TE = trailing edge

References

AQ3 [1] Camfil FARR, 2013, Technical Report No. ■.

[2] Kurz, R., Brun, K., Meher-Homji, C., and Moore, J., 2012, "Gas Turbine Performance and Maintenance," Proceedings of the Forty-First Turbomachinery Symposium, Houston, TX. AQ4

[3] Hanhui, J., Chao, H., Lin, L., and Jianren, F., 2013, "Numerical Investigation of the Wall Effect on Airborne Particle Dispersion in a Test Chamber," Aerosol Air Qual. Res., **13**, pp. 786–794.

[4] Wilcox, M., Kurz, R., and Brun, K., 2012, "Successful Selection and Operation of Gas Turbine Inlet Filtration Systems," Proceedings of the Fortieth Turbomachinery Symposium, Houston, TX.

[5] Heim, L. O., Blum, J., Preuss, M., and Butt, H. J., 1999, "Adhesion and Friction Forces between Spherical Micrometer-Sized Particles," Phys. Rev. Lett., **83**(16), pp. 3328–3331.

[6] Suman, A., Kurz, R., Aldi, N., Morini, M., Brun, K., Pinelli, M., and Spina, P. R., 2014, "Quantitative CFD Analyses of Particle Deposition on a Transonic Axial Compressor Blade, Part I: Particle Zones Impact," ASME Paper No. GT2014-25282.

[7] Hertz, H., 1882, "Uber die Beriihrung Fester Elastischer Korper," J. Reine Angew. Math., **92**, pp. 156–171 [Jones, D. E., and Schott, G. A., 1896, "Miscellaneous Papers by H. Hertz," Macmillan, London (in English)]. AQ5

[8] Johnson, K. L., Kendall, K., and Roberts, A. D., 1971, "Surface Energy and the Contact of Elastic Solids," Proc. R. Soc. London, Ser. A, **324**(1558), pp. 301–313.

[9] Thornton, C., and Ning, Z., 1998, "A Theoretical Model for the Stick/Bounce Behavior of Adhesive Elastic-Plastic Spheres," Powder Technol., **99**(2), pp. 154–162.

[10] Wall, S., John, W., Wang, H. C., and Goren, S. L., 1990, "Measurements of Kinetic Energy Loss for Particles Impacting Surfaces," Aerosol Sci. Technol., **12**(4), pp. 926–946.

[11] Poppe, T., Blum, J., and Henning, T., 2000, "Analogous Experiments on the Stickiness of Micron-Sized Preplanetary Dust," Astrophys. J., **533**(1), pp. 454–471.

[12] Poppe, T., and Blum, J., 1997, "Experimental on Pre-Planetary Grain Growth," Adv. Space Res., **20**(8), pp. 1595–1604.

[13] Hamed, A., Tabakoff, W., and Wenglarz, R., 2006, "Erosion and Deposition in Turbomachinery," J. Propul. Power, **22**(2), pp. 350–360.

[14] Hamed, A. A., Tabakoff, W., Rivir, R. B., Das, K., and Arora, P., 2005, "Turbine Blade Surface Deterioration by Erosion," ASME J. Turbomach., **127**(3), pp. 445–452.

[15] Suzuki, M., Inaba, K., and Yamamoto, M., 2008, "Numerical Simulation of Sand Erosion Phenomena in Rotor/Stator Interaction of Compressor," J. Therm. Sci., **17**(2), pp. 125–133.

[16] Ghenaiet, A., 2012, "Study of Sand Particle Trajectories and Erosion Into the First Compression Stage of a Turbofan," ASME J. Turbomach., **134**(5), p. 051025.

[17] Reid, L., and Moore, R. D., 1978, "Design and Overall Performance of Four Highly-Loaded, High-Speed Inlet Stages for an Advanced High-Pressure-Ratio Core Compressor," NASA TP 1337.

[18] ANSYS FLUENT, 2010, Release 13.0.

[19] Ahlert, K., 1994, "Effects of Particle Impingement Angle and Surface Wetting on Solid Particle Erosion of AISI 1018 Steel," M.S. thesis, Department of Mechanical Engineering, The University of Tulsa, Tulsa, OK.

[20] Forder, A., Thew, M., and Harrison, D., 1998, "A Numerical Investigation of Solid Particle Erosion Experienced Within Oilfield Control Valves," Wear, **216**(2), pp. 184–193.

[21] Kurz, R., and Brun, K., 2012, "Fouling Mechanism in Axial Compressors," ASME J. Eng. Gas Turbines Power, **134**(3), p. 032401.

[22] Mangwandia, C., Cheonga, Y. S., Adamsb, M. J., Hounslowa, M. J., and Salmana, A. D., 2007, "The Coefficient of Restitution of Different Representative Types of Granules," Chem. Eng. Sci., **62**(1–2), pp. 437–450.

[23] Adi, S., Adi, H., Chan, H.-K., Tong, Z., Yang, R., and Yu, A., 2013, "Effects of Mechanical Impaction on Aerosol Performance of Particles With Different Surface Roughness," Powder Technol., **236**, pp. 164–170. AQ6

[24] Silingardi, A., Astrua, P., Piola, S., and Ventrucci, I., 2013, "A Method for a Reliable Prediction of Heavy Duty Gas Turbines Performance Degradation due to Compressor Aging Employing Field Test Data," Power Gen Europe, Messe, Wien, Austria.

[25] Morini, M., Pinelli, M., Spina, P. R., and Venturini, M., 2011, "Numerical Analysis of the Effects of Non-Uniform Surface Roughness on Compressor Stage Performance," ASME J. Eng. Gas Turbines Power, **133**(7), p. 072402.